THE EFFECT OF REALISTIC GEOLOGIC HETEROGENEITY ON LOCAL AND REGIONAL P/S AMPLITUDE RATIOS BASED ON NUMERICAL SIMULATIONS

Stephen C. Myers[1], Jeffery Wagoner[1], Leiph Preston[2], Ken Smith[2], and Shawn Larsen[1]

Lawrence Livermore National Laboratory[1] and University of Nevada at Reno[2]

Sponsored by National Nuclear Security Administration
Office of Nonproliferation Research and Engineering
Office of Defense Nuclear Nonproliferation

Contract Nos. W-7405-ENG-48[1] and DE-FC03-02SF22656[2]

ABSTRACT

Regional seismic discriminants based on high-frequency P/S ratios reliably distinguish between earthquakes and explosions. However, P/S discriminants in the 0.5 to 3 Hz band (where the signal-to-noise ratio [SNR] can be highest) rarely perform well, with similar ratios for earthquake and explosion populations. Variability in discriminant performance has spawned numerous investigations into the generation of S-waves from explosions. Several viable mechanisms for the generation of S-waves from explosions have been forwarded, but most of these mechanisms do not explain observations of frequency-dependent S-wave generation. Recent studies have focused on the effect of near-source scattering to explain the frequency-dependence of both S-wave generation and P/S discriminant performance. In this study we investigate near-source scatter through numerical simulation with a realistic geological model.

We have constructed a realistic, three-dimensional (3D) earth model of the southern basin and range. This regional model includes detailed constraints at the Nevada Test Site (NTS) based on extensive geologic and geophysical studies. Gross structure of the crust and upper mantle is taken from regional surface-wave studies. Variations in crustal thickness are based on receiver function analysis and a compilation of reflection/refraction studies. Upper-crustal constraints are derived from geologic maps and detailed studies of sedimentary basin geometry throughout the study area. The free surface is based on a 10-m digital elevation model (DEM) at NTS, and a 60-m DEM elsewhere. The model extends to a depth of 150 km, making it suitable for simulations at local and regional distances.

Our simulation source is based on the 1993 non-proliferation experiment (NPE) explosion at NTS. This shot was well recorded, offering ample validation data. Our validation tests include measures of long-period waveform fit and relative amplitude measurements for P and S phases. Our primary conclusion is that near-source topography and geologic complexity in the upper crust strongly contributed to the generation of S-waves from the NPE shot. When either geologic heterogeneity or topography is removed from the model, simulated amplitudes of regional S-waves are diminished. We also find that deeper sources scatter less energy off of topography and upper-crustal structures, resulting in diminished S-wave amplitudes with increasing source depth.

OBJECTIVE

Regional monitoring relies heavily on comparisons of P- and S-phase amplitudes (Pomeroy et al., 1982; Walter et al., 1995). Further, widely used methods of determining magnitude make use of Lg and Lg coda amplitudes (e.g., Nuttli, 1986; Mayeda and Walter, 1996; Patton, 2001), and regional S-phases often add important arrival-time observations to limited, small-magnitude data sets used for location (Denny and Stull, 1994; Mayeda and Waltr, 1996; Myers et al., 1999).

Most investigators agree that appreciable energy from the explosions is converted to S-waves near the source, but the dominant P-to-S transfer mechanism is not agreed upon. Several physically reasonable transfer mechanisms are proposed, including P-to-S conversion at the free surface, spall, scattering of short-period surface waves, tectonic release, and rock-damage (e.g., Vogfjord, 1997; Day and Mclaughlin, 1991; Gupta et al., 1992; Wallace et al., 1985; Johnson and Sammis, 2001). Each mechanism fits a subset of observations, and each mechanism, with the exception of surface-wave scattering, is understood from first principles. Currently, the Rg-to-S mechanism is represented by an empirical transfer function (e.g., Gupta et al., 1992; Patton, 2001).

This project aims to study the physical process of near-source scattering to establish a fundamental understanding of this phenomenon. Our recent progress is in the area of model construction, and subsequent numerical experiments on the effect of near-source topography and event depth are presented below.

RESEARCH ACCOMPLISHED

In previous years of this project, we developed a detailed upper-crustal model centered on the 1993 NPE shot (Figure 1). The rationale for centering on the NPE is discussed in the subsection, “Model validation using NPE observations.” The local model is 20 km on a side (including depth), and construction of the model leverages the extensive Lawrence Livermore National Laboratory (LLNL) database of geological and geophysical information that includes mapping, bore-hole logs, seismic surveys, and gravity surveys (e.g., Healey et al., 1963). Much of LLNL’s geological database is unpublished. The local model is imbedded in a regional model that will allow simulations to distances of interest.

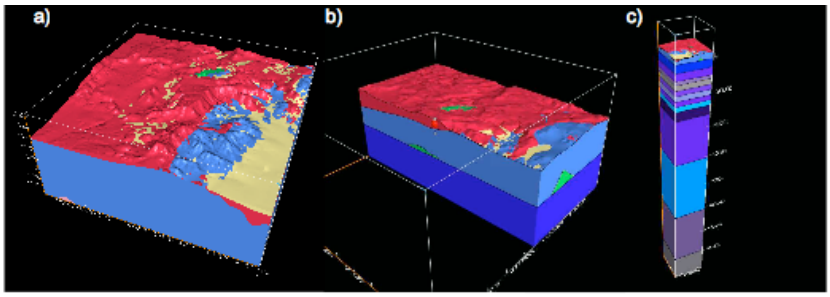

Figure 1. Local model around NPE shot determined from detailed geologic and geophysical studies. (a) The entire local model. (b) Cross section through the NPE shot. (c) Local model merged into a lithospheric velocity stack.

We have made considerable advances this year in the regional model (Figure 2). The default velocity structure continues to be a one-dimensional (1D) model based on work of Patton and Taylor (1984). Variations to the default model are based on the geographic specifics of published studies. The current version of the model includes variations in upper-crustal structure based on regional geologic maps of Nevada, Utah, California, and Arizona. We assume that crystalline rocks are continuous into the lower crust and that basin depths are proportional to the magnitude of local gravity anomalies (e.g., Blakely et al., 1997). The lower crustal velocities and Moho depth are modified based on the work of Zandt et al. (1994) and Mooney et al. (1998). Minor modifications to mantle velocities are based on refraction profiles summarized in Mooney et al. (1998). In specific areas we have incorporated tomographic studies, such as Biasi (2005) and Preston et al. (2005).

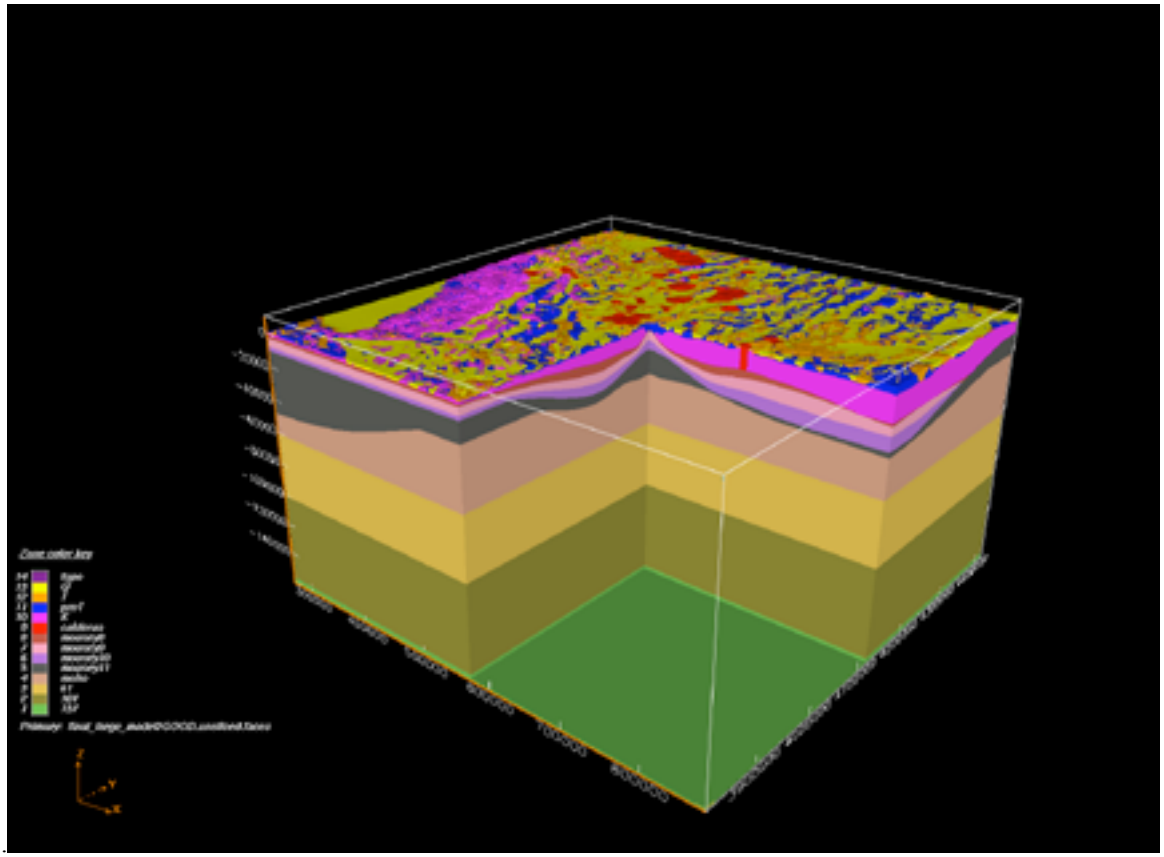

Figure 2. Regional geologic model centered on NTS. The model extends into California (to the left) and Utah and Arizona (to the right). The model is a compilation of geologic mapping; seismic profiles, receiver functions, and tomography; and gravity modeling for basin structure.

Model validation using NPE observations

We use the E3D code of Larson and Grieger (1998) for seismic simulations. E3D is a full elastic code that allows the input of a general geologic structure, including the free surfaces. All of our simulations use a grid spacing of 60 m, which enables interpretation to 3 or 4 Hz.

Our numerical simulations are based on the 1993 NPE. The NPE was a 1-kiloton chemical explosion at NTS. NPE details and research reports can be found in Denny and Stull. (1994). Figure 3 shows the extensive network of stations that recorded the NPE. We have compiled all these recordings to validate our model. We begin with the local recordings, which we used both to validate the near-source model and to estimate the NPE moment tensor.

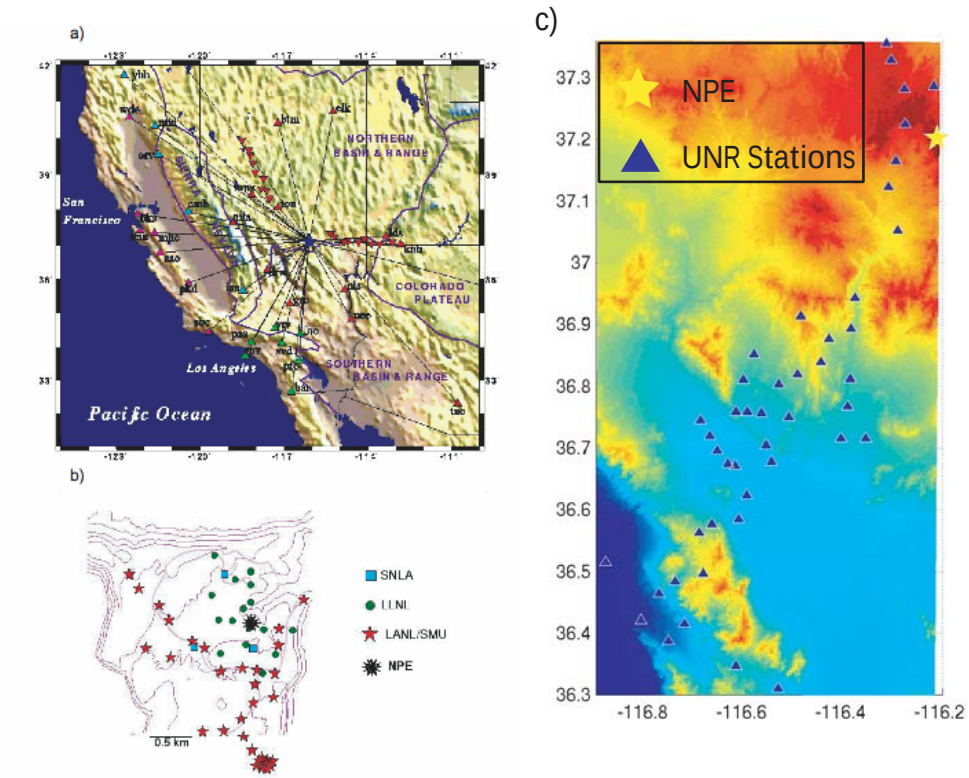

Figure 3:Stations with recordings of the NPE shot. We have compiled waveforms from all of these stations.

Figure 4 shows an example waveform (black) from a station that is approximately 2 km from the NPE. Simulations (red) with combinations of isotropic (Figure 4 a,b) and CLVD (Figure 4 c,d) moment tensors and topographic free surface (Figure 4 a,c) and flat free surface (Figure 4 b,d) are compared with the data. It is clear that the isotropic source in a model that includes the topographic free surface is the best fit to the data. Comparisons with other local data (not shown) are similar, and we conclude that the NPE is best modeled as an isotropic source.

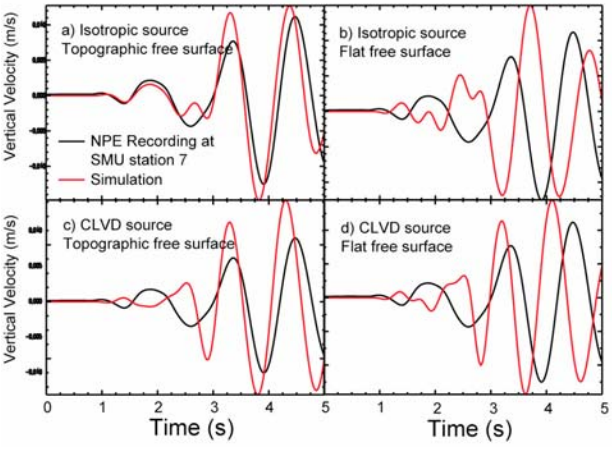

Figure 4. Recorded (black) and simulated (red) displacement seismograms for the NPE shot. These 3-dimensional simulations make use of the local NPE model (see above). Event-station distance is approximately 2 km. a) simulation with isotropic moment tensor and free surface based on digital elevation model (DEM). b) Simulation with isotropic source and flat free surface. c) Simulation with compensated linear vector dipole (CLVD) moment tensor with DEM free surface. d) Simulation with CLVD moment tensor and flat free surface. The NPE is best modeled as an isotropic source. Simulation with a realistic free surface is essential to match the data.

We also conclude that simulations that include the frequencies of interest (up to 3-4 Hz) must include a realistic topographic model.

Figure 5 is an example of our regional validation effort, which is on-going. In this example we use the temporary, broadband (STS-2 sensor) deployment fielded by the University of Arizona. The cross section is color coded to P-wave velocity, which was taken from our regional 3-dimensional model. The upper crust is characterized by Paleozoic sedimentary rocks, which are interrupted by low-velocity basins. Velocity in the mid- and lower crust primarily increases with depth, but we include minor lateral variation in velocity as well has changes in Moho depth based on the work of Zandt et al. (1995). The interface between light and dark red in the lower quarter of the cross section is the Moho. We have superimposed a snap shot of the seismic wavefield on the cross section to demonstrate the complexity that results from this relatively simple model.

The traces shown in Figure 5 compare recorded (black) and synthetic (red) velocity seismograms. Both velocity and synthetic records are band passed between 0.7 Hz and 3 Hz. Amplitudes are normalized because geometric spreading in the 2-dimensional synthetics is incorrect. In general, the comparison of observed and synthetic data is favorable. The degree of waveform complexity is nearly identical, and it would be difficult to tell which trace is real based on simple inspection. The relative amplitudes of the real and synthetic waveforms are also in good agreement (with the notable exception of sta 8, where synthetic amplitudes after the first arrival are too large). Although the phase is matched in many instances (particularly the first arrival), we cannot claim to have simulated phase reliably. Nonetheless, the overall agreement between observed and synthetic data is very good, especially considering that the model was not directly derived from the data.

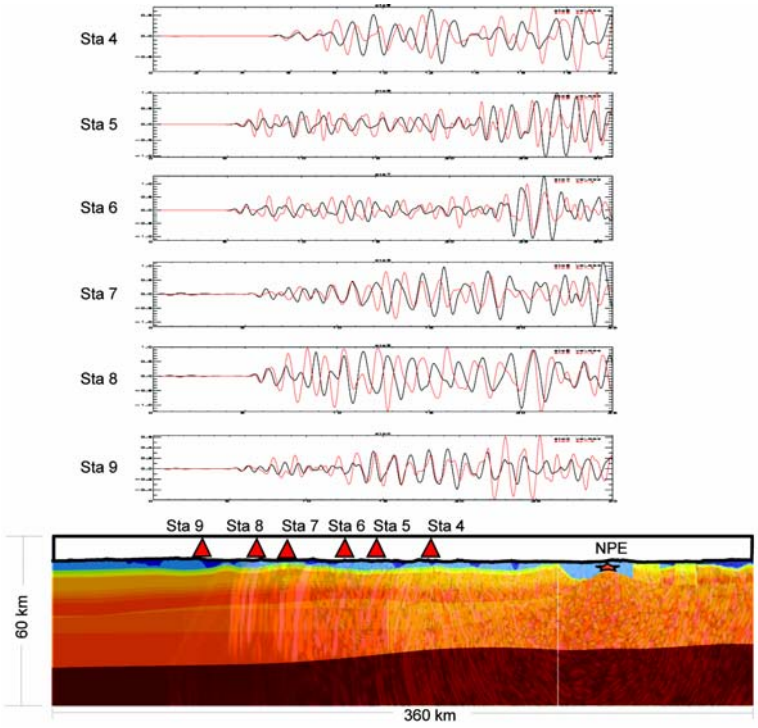

Figure 5. Model validation with regional seismic simulations of the U. Arizona broadband deployment (line extending east from NPE in Figure 3). West is to the right. Lower cross-section shows a snap shot of the seismic wavefield overlain on a P-wave velocity. The transition from red to near black in the lower quarter of the cross section is the Moho. The cross section and waveform are for the station 9 simulation. A separate 2-dimensional simulation was made for each of the stations to account for azimuth variations in structure. The upper traces are vertical velocity recordings of the NPE between 0.7 Hz and 3 Hz (black) with synthetics (red) for comparison. Amplitudes are normalized. Note that the time windows for the different stations are not synchronized. The general character of the observed seismograms is duplicated by the synthetics, suggesting that the regional model is a reasonable rendition of true structure.

The effect of topography on P/S ratios

Figure 6 is a map-view snap shot of a local simulation with and without topography (note that these are the same simulation that produced the synthetic seismograms in Figure 4 a,b). The topographic elevation at the NPE epicenter is used as the reference elevation for the flat free surface simulations. Topography that lies below that reference has surface velocity extended to the level of the reference; topography that extends above the reference is truncated at the reference level. Figure 6 shows that local topography immediately imparts disorder (scattering) into the wavefield.

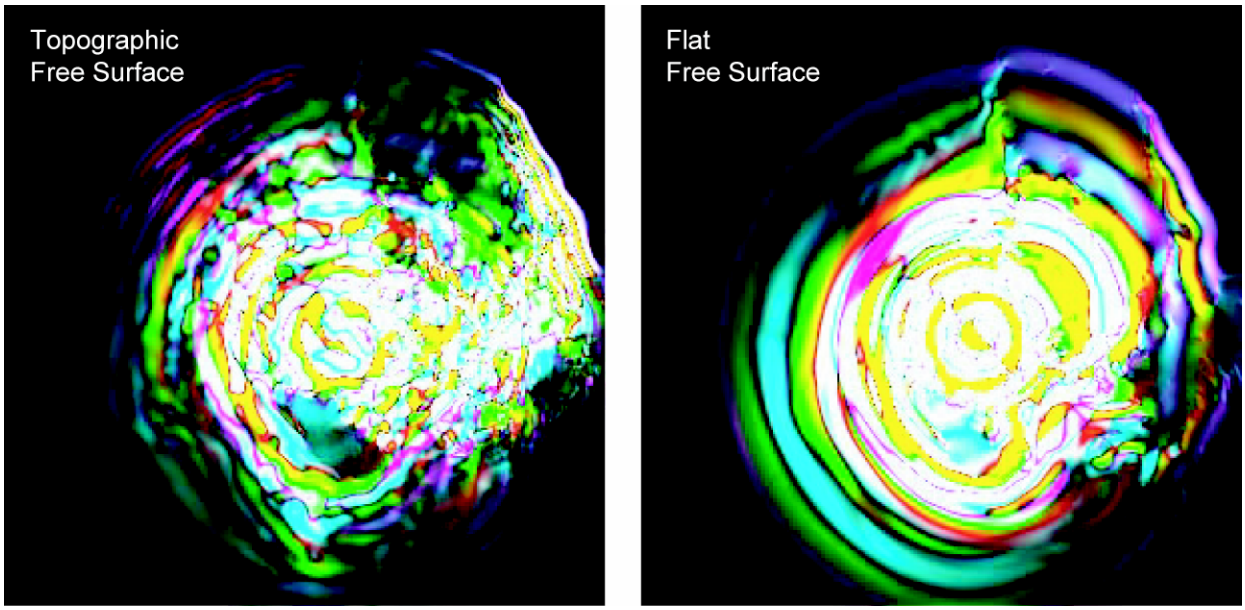

Figure 6. Map view of simulations with topographic free surface based on a digital elevation model (left) and flat free surface (right). Red, magenta and blue colors are P-waves. Green and yellow colors are S-waves. The map views shown above are 20 km on a side. Images are snap shots at approximately 5.5 seconds after event origin time and are at the lowest topographic elevation in the model. Detailed geologic structure from local mapping and geophysical studies is included in both simulations. Inclusion of realistic topography complicates the wave field considerably with appreciably more scattering.

Figure 7 shows synthetic spectra and seismograms of P-potential and S-potential at approximately 5 km from the source (Taken from the simulations shown in Figure 4). In all cases the S-potential exceeds the P-potential, which is presumably the result of free surface effects. However, the real topographic free surface results in a frequency-dependent P/S ratio. In fact the P/S ratio is significantly decreased at frequencies close to 1 Hz. Although these results are preliminary, the qualitative similarity in the frequency dependence of observed P/S ratios (mentioned in the Objectives section) and the synthetic P/S ratios for simulations that include real topography is suggestive. Further testing and rigor will determine whether topographic scattering is the primary mechanism for S-waves in the 1 Hz band.

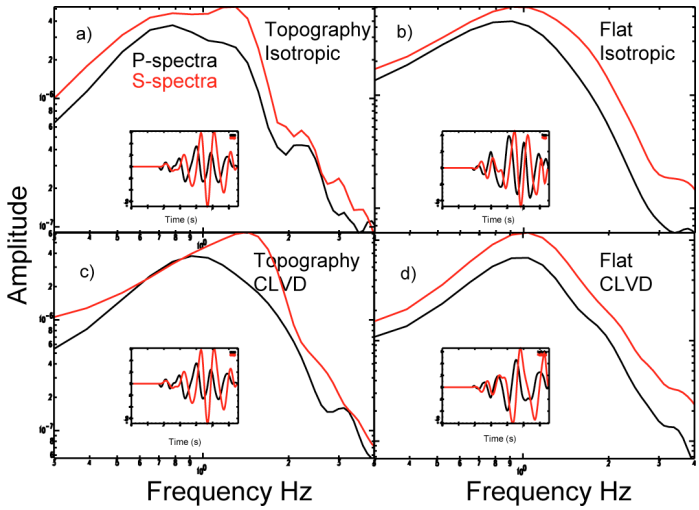

Figure 7. P (black) and S (red) displacement spectra and seismograms for simulations of the NPE shot (simulations shown in Figure 4). These 3-dimensional simulations make use of the local NPE model (see above). The inset seismograms are P-potential (black) and S-potential (red) for a location approximately 5 km from the source. The spectra are derived from P and S potential seismograms. (a) Simulation with isotropic moment tensor and free surface based on DEM. (b) Simulation with isotropic source and flat free surface. (c) Simulation with CLVD moment tensor with DEM free surface. (d) Simulation with CLVD moment tensor and flat free surface. Both isotropic and CLVD moment tensors produce a distinctly frequency-dependent P/S ratio.

The effect of source depth on P/S ratios

Results presented above suggest that near-source scattering, particularly scattering off of the free surface, boosts the amplitude of radiated S-waves at the expense of P-wave amplitudes. We test this hypothesis by comparing the simulation of a shallow source with a simulation of a deep (mid-crustal) source (Figure 8). Near-source heterogeneity for the shallow source (upper-crustal structure and topography) is considerable. Near-source heterogeneity for the deep source, where velocity is changing smoothly with depth, is minor. In both instances the source is isotropic (explosion) with the same moment. The model is approximately 300 km wide and 150 km deep. Some artifacts from reflections off of the side of the model are evident, but these artifacts do not muddle the overall picture.

The difference between the shallow- and deep-source simulations is striking. For the shallow source, S-waves grow to large amplitudes within seconds. The large S-waves radiate from the source in all directions. Therefore, S-waves are observed to propagate at steep angles into the mantle (and could propagate to teleseismic distances), as well as at shallow angles into the crustal waveguide to regional distances. For the deep source, S-waves are all but absent until the P-wave enters the upper crust. Notable conversion to S-waves does occur, but the S-wave amplitudes are significantly smaller than they are for the shallow source. Much of the S-wave energy is trapped in the upper crust, forming a P-coda. S-energy that escapes local, upper-crustal structures (e.g., basins) is reflected downward at steep angles. Therefore, the majority of the S-energy that escapes the upper crust is transmitted into the mantle, and little energy is trapped in the crustal waveguide.

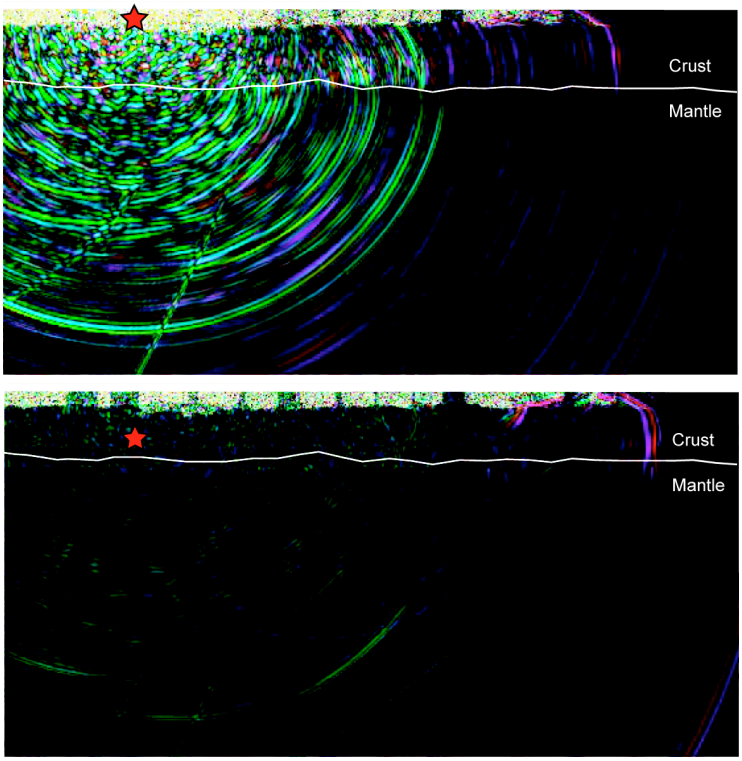

Figure 8. Regional 2D simulation showing the difference between a shallow source (upper panel) and a deep source (lower panel). The red star shows the source location. The model is approximately 300 km wide and 150 km deep. Both snapshots are at approximately 75 s after the source origin time. The shallow source generates vastly more S-waves (green and yellow) than the deeper source. The intensity of Pg (red and blue crustal phase on the right side of each panel) is greater for the deeper source.

CONCLUSIONS AND RECOMMENDATIONS

We have constructed a regional model centered on the NTS based on published and unpublished studies. The starting point of the regional model is a 1D model that is based on surface-wave studies. We include significant 3D modifications to the 1D model based on receiver function, refraction, reflection, and gravity studies. The regional model includes a detailed upper-crustal model centered on the NPE explosion. This local model is constrained by geologic maps, borehole data, and geophysical studies at the NTS. The local model is seamlessly imbedded into a regional model to enable realistic simulations of NTS sources to regional distance.

Validation of the model is based on recordings and simulations of the NPE shot. Validation of the local model is complete and the model reliably predicts local NPE waveforms. Validation of the regional model is ongoing, and we are reliably predicting the character of regional waveforms (i.e., arrival times and relative amplitudes of regional phases). However, accurate prediction of the full waveform (including phase) is spotty.

Local 3D simulations demonstrate that topographic scattering is an important source of S-wave generation for the NPE. We find that topographic scattering peaks S-wave amplitudes at approximately 1 Hz, which is in agreement with observations in many instances (at NTS and other locales). Topographic scattering produces a disordered wavefield and scatters energy in all directions. Simulations with a flat free surface produce S-waves, but little frequency dependence is observed.

Regional simulations demonstrate that a shallow NPE source produces appreciable S-waves that radiate at a large range of slownesses. For shallow sources, S-waves generated through structural and topographic scattering propagate in all directions. This means that the S-wave propagate at steep angles into the mantle (and would

presumably continue to teleseismic distance) as well as into the regional waveguide to form Sn and/or Lg. When the equivalent NPE source is placed in the mid-crust, S-wave generation is significantly diminished. S-waves are generated as the P-wave traverses the upper crust and reflects off of the topographic free surface, but S-waves that escape the upper crust travel at steep angles and are largely transmitted into the mantle.

ACKNOWLEDGEMENTS

We acknowledge the LLNL containment program for generous access to its extensive database of geologic and geophysical studies at NTS. We also would like to thank Glenn Biasi and Walter Mooney for providing regional geophysical information.

REFERENCES

Blakely, R. J., R. C. Jachens, J. P. Calzia, and V. E. Langenheim (1997), Cenozoic Basins of the Death Valley Extended Terrain as Reflected in Regional-Scale Gravity Anomalies, in Wright, L.A. and B.W. Troxel, Eds., Cenozoic Basins of the Death Valley Region, *Geol. Soc. Am. Special Paper* 333.

Biasi, G. (2005), Mantle Lithospheric Clues to Walker Lane Evolution, 2005 Seismological Society of America spring meeting, Incline, NV.

Day, S. and K. Mclaughlin (1991), Seismic Source Representations for Spall, *Bull. Seismol. Soc. Am*. 81: 191–201.

Denny, M. D. and S. P. Stull, Eds. (1994), *Proceedings of the Symposium on the Non-Proliferation Experiment (NPE): Results and Implications for Test Ban Treaties*, Lawrence Livermore National Laboratory CONF-9404100.

Glenn L. and S. Myers (1997). Depth of Burial Experiment at Balapan, in *Proceedings of the International Symposium on Monitoring and Discrimination of Underground Nuclear Explosions and Earthquakes*, Lawrence Livermore National Laboratory UCRL-JC-1283 13: 229–235.

Gupta, I. N., W. W. Chan, and R. A. Wagner (1992), A Comparison of Regional Phases from Underground Nuclear Explosions at East Kazakh and Nevada Test Site, *Bull. Seismol. Soc. Am*. 82: 352–382.

Gupta, I. N., T. R. Zhang, and R. A. Wagner (1997), Low Frequency Lg from NTS and Kazakh Nuclear Explosions—Observations and Interpretations, *Bull. Seismol. Soc. Am*. 87, 1115–1125.

Healey, D. L. and Miller, C. H. (1963), Gravity Survey of the Gold Meadows Stock, Nevada Test Site, Nye County, Nevada, USGS Technical Letter NTS-40.

Jih, R. S. (1995), Numerical Investigation of Relative Contribution of Rg Scattering and Incomplete Dissipation to Lg Excitation, in *Proceedings of the 17th Seismic Research Symposium on Monitoring a Comprehensive Test Ban Treaty*, PL-TR-95-2108, 1: pp. 401–410.

Johnson, L. R. and C. G. Sammis (2001), Effects of Rock Damage on Seismic Waves Generated by Explosions, *Pageoph* 158: 1869-–908.

Larsen, S. C. and C. A. Schultz, ELAS3D: 2D/3D Elastic Finite-Eifference Wave Propagation Code, LLNL internal report, 18.

Larsen, S. and J. Grieger (1998), Elastic Modeling Initiative, Part III: 3-D Computational Modeling, in *Proceedings of the Society of Exploration Geophysicists International Conference* 68: pp. 1803–1806.

Levander, A. R. (1988), Fourth-Order Finite-Difference P-SV Seismograms, *Geophysics* 53: 1425–1436

Mayeda, K. and W. Walter (1996). Moment, Energy, Stress Drop, and Source Spectra of Western United States Earthquakes from Regional Coda Envelopes, *J. Geophys. Res*. 101: 11,195–11,208.

Myers, S. C., W. R. Walter, K. Mayeda, and L. Glenn (1999), Observations in Support of Rg Scattering as a Source for Explosion S Waves: Regional and Local Recordings of the 1997 Kazakhstan Depth of Burial Experiment, *Bull. Seismol. Soc. Am*. 89: 544–549.

Myers, S. C., D. B. Harris, M. L. Anderson, W. L. Rodi, W. R. Walter, M. P. Flanagan, and F. Ryall, LLNL Location and Detection Research 2003, in *Proceedings of the 25th Seismic Research Review—Nuclear Explosion Monitoring: Building the Knowledge Base*, LA-UR-03-6029, 1: pp. 259–268.

Mooney, W., G. Laske, G. Masters (1998), Crust 5.1: A Global Crustal Model at 5 × 5 Degrees, *J. Geophys. Res*. 103: 727–747.

Nuttli, O. W. (1986), Yield Estimates of Nevada Test Site Explosions Obtained from Seismic Lg Waves, *J. Geophys. Res*. 91: 2137–2151.

Patton, H. J. and S. R. Taylor (1984), Q-Structure of the Basin and Range from Surface Waves, *J. Geophys. Res*. 89 (NB8): 6929–6940.

Patton, H. J. (2001), Regional Magnitude Scaling, Transportability, and Ms:mb Discrimination at Small Magnitudes, *Pageoph* 158: 1951–2015.

Pomeroy, P., W. Best, and T. McEvilly (1982), Test Ban Treaty Verification with Regional Data—A Review, *Bull. Seismol. Soc. Am*. 72: S89–S129.

Preston, L., K. Smith, and D. von Seggern (2005), 3D Velocity Structure of the Yucca Mountain, 2005 Seismological Society of America Meeting, Incline, NV.

Stevens, J. L., G. E. Baker, H. Xu, T. J. Bennett, N. Rimer, and S. M. Day (2004), The Physical Basis of Lg Generated by Explosion Sources, in *Proceedings of the 26th Seismic Research Review: Trends in Nuclear Explosion Monitoring*, LA-UR-04-5801.

United States Geological Survey (1983), Geologic and Geophysical Investigations of Climax Stock Intrusive, Nevada, USGS Open-File Report 83-377.

Vogfjord, K. (1997), Effect of Explosion Depth and Earth Structure on the Excitation of Lg Waves: S* Revisited, *Bull. Seismol. Soc. Am*. 87: 1100–1114.

Walter, W., K, Mayeda, and H. Patton (1995), Phase and Spectral Ratio Discrimination between NTS Earthquakes and Explosions, Part I: Empirical Observations, *Bull. Seismol. Soc. Am*. 85: 1050–1067.

Walter, W. R., K. Mayeda, and H. J. Patton, Regional Seismic Observations of the Non-Proliferation Experiment at the Livermore NTS Network, in *Proceedings of the Symposium on The Non-Proliferation Experiment (NPE): Results and Implications for Test Ban Treaties*, M. D. Denny and S. P. Stull, Eds.

Whitney, J. W. and W.R. Keefer, Geologic and Geophysical Characterization Studies of Yucca Mountain, Nevada, a Potential High-Level Radioactive-Waste Repository, *USGS Digital Data Series* 58.

Wu, R. S., X. B. Xie, Z. Ge, and T. Lay (2004), Quantificating Source Excitation and Path Effects for High Fequency Regional Waves, in *Proceedings of the 26th Seismic Research Review: Trends in Nuclear Explosion Monitoring*, LA-UR-04-5801.

Zandt, G., S. C. Myers, and T. C. Wallace (1995), Crust and Mantle Structure across the Basin and Range—Colorado Plateau at 37° North Latitude and Implications for Cenozoic Extension Mechanism, *J. Geophys. Res*. 100: 10,592–10,548.